Article

Mechanical Properties and Residual Stress Measurement of TiN/Ti Duplex Coating Using HiPIMS TiN on Cold Spray Ti

Nhat Minh Dang [1], Wen-Yen Lin [2], Zhao-Ying Wang [1], Sima Ahmad Alidokht [3], Richard R. Chromik [3], Terry Yuan-Fang Chen [4] and Ming-Tzer Lin [1,5,*]

[1] Graduate Institute of Precision Engineering, National Chung Hsing University, Taichung 40749, Taiwan; d108067005@mail.nchu.edu.tw (N.M.D.); d108067002@mail.nchu.edu.tw (Z.-Y.W.)
[2] Taiwan Semiconductor Manufacturing Co., Ltd., Hsinchu Science Park, Hsinchu 300096, Taiwan; willylin710@gmail.com
[3] Department of Mining and Materials Engineering, McGill University, Montreal, QC H3A 0C5, Canada; sima.ahmadalidokht@mail.mcgill.ca (S.A.A.); richard.chromik@mcgill.ca (R.R.C.)
[4] Department of Mechanical Engineering, National Cheng Kung University, Tainan 70101, Taiwan; ctyf@mail.ncku.edu.tw
[5] iCenter for Advanced Science Technology, National Chung Hsing University, Taichung 402, Taiwan
* Correspondence: mingtlin@nchu.edu.tw; Tel.: +886-4-2285-3828

Abstract: This study investigated the mechanical properties and the residual stress of high-power impulse magnetron sputtering (HiPIMS) titanium nitride (TiN) thin film capping on cold spray titanium (Ti) coating. This TiN/Ti duplex coating was deposited on the Ti substrate, and the cold spray titanium (Ti) coating was prepared in three cases with different numbers of layers. The study determined Young's modulus, hardness, and roughness of TiN thin film and cold spray Ti coatings by nano-indentation and AFM. The residual stress measurement of TiN/Ti duplex coating was conducted using the ring-core drilling method. A focused ion beam (FIB) drilled the TiN/Ti duplex coating with various milling depth steps. The corresponding images were obtained with a scanning electron microscope (SEM). The relationship between surface deformations and relaxation stress after each milling depth step was obtained using the digital image correlation (DIC) method. The results showed TiN/Ti duplex coating exhibited excellent mechanical properties, and the residual stresses were not significantly changing with different Ti cold spray substrates, showing the feasibility of coating technology for the future applications in the aerospace industry.

Keywords: residual stress; focused ion beam (FIB); digital image correlation (DIC); high power impulse magnetron sputtering (HiPIMS); duplex coatings; Ti cold spray

1. Introduction

In the aerospace industry, the engines, compressor blades of turbine engines, and surfaces of airplanes and propellers are components frequently operated in harsh environments, which predispose them to surface damage and erosion [1,2]. To lessen this, the cold spray film technology is used to create a protective coating of an anti-erosion material. Cold-sprayed coatings are a newly developed technology used to build industrial components because of the applicability of this process in production technology [3–5]. This technology can be an attractive alternative to traditional thermal-spray techniques because it is performed at low temperatures. The cold-spray process will not significantly affect or change the properties of the material such as the micro or nanostructure of metals, including Ti. In general, the advantages of cold spray materials include increasing the resistance of the protective coating to deformation through its high coating density and extensive grain refinement, improving the hardness and enhancing the residual compressive stresses.

In recent years, high-power impulse magnetron sputtering (HiPIMS) has been proven to have considerable versatility in fabricating specially designed micro and nanostructured

thin-film coatings. The typical sputtering region in HiPIMS is between 10 μs and 200 μs, with a total pulse width of 20 ms to 40 ms [6,7]. These short impulses carry a high peak power density of up to a few kilowatts per square centimeter and are dissipated on the target material to generate a large number of ions in the plasma [8,9]. Previous studies have demonstrated that the quality of the component surface has a close relationship with the ionic effect in the HiPIMS process [10–12]. This indicates that there is a continuous plasma chemical change at regular intervals of the impulses, which further improves the coating properties. Further, it has been shown that accurate control of phase composition in the coating can help crystalline grains grow in the preferred orientation [13], with micro/nanostructures having a tight atomic density; more importantly, it was found that it can grow coatings at a low temperature [14]. Cold-sprayed plus HiPIMS multiple thin films have become a very prominent coating application for modern industrial development.

High-quality TiN thin films are widely used in the aerospace industry, ranging from hard and protective coatings on components made of Ti to the barrier in components of the engines. Previously, D. Goldbaum et al. [1] carried out a complete study on the tribological behavior of TiN and Ti (Si, C)N coatings on cold-sprayed Ti substrates. It provided a proof of concept for TiN coatings on cold sprayed Ti substrates. Despite its prominent tribological behavior, the residual stress of TiN/Ti duplex coating remains unknown. The residual stress of the TiN thin film on the cold-sprayed Ti coating can be changed with different thin film deposition processes as well as cold spray coating processes. If the residual stress was too high, it may result in surface erosion, cracks, or damage.

In terms of the residual stress, the analysis of residual strain depth profiles requires detailed knowledge of the in-depth lattice strain function because the residual stress profile calculation must consider the mechanical anisotropy and texture of the materials. The traditional application of X-ray diffraction techniques to the residual stress analysis in amorphous materials is often not possible. The development of a microstructure-independent procedure for the depth-resolved measurement of residual stress is an issue of strategic interest. In particular, no techniques are currently available that can produce a sub-micron lateral and depth resolution in an automated and robust manner. In this research, it was assumed that these limitations could be surmounted through the use of a combination of FIB milling, SEM imaging, DIC analysis, and finite element modeling [15–19]. Thus, the study provides important information on residual stress measurement of the thin film through PVD, sputter, and HiPIMS.

The objective of this study was to investigate the mechanical properties and residual stress of the combination of protective hard coatings (TiN/Ti duplex coating) deposited through HiPIMS on top of the three different cold-sprayed Ti grade 4 coatings deposited on the conventional Ti grade 12 substrates [20]. The residual stress of HiPIMS TiN film measured by THE FIB–DIC method [15] on top of three different cold spray Ti coatings was able to predict the influence of the substrate effects on the mechanical behavior of TiN/Ti duplex coating using HiPIMS TiN on cold-sprayed Ti coating. This study would benefit the industry since cold spraying is cost-saving, sustainable, and has low environmental impacts.

2. Experimental Procedure

2.1. Ti Cold-Spray Deposition

The cold-spray coating, called the adhesion coating, was located between TiN thin film and Ti grade 12 substrates [20]. The adhesion coating (thickness of 5 mm, different number of layers) was produced in three types: two layers (2p), eight layers (8p), and 14 layers (14p). The cold-spray deposition was carried out using a Plasma Giken PCS 1000 cold-spray gun equipment (Plasma Giken Co., Yorii, Saitama, Japan) performed at the National Research Council (NRC) Boucherville, Canada. Figure 1 shows the schematic diagram of the cold-spray system. Prior to deposition of the coating, the Ti grade 12 substrates were grit blasted and cleaned (see Figure 2a). The gas temperature and pressure of the propellant gas of the spray gun were set and maintained during the fabrication of the experimental samples. Stand distance, movement speed, and feed rate were flexibly adjusted to obtain the target

number of layers and thickness. As shown in Figure 2c, after preparing the adhesion coating process, cubes with 1 cm³ were cut using a Buehler Ismet 5000 Linear Precision Saw. The cold-sprayed cubes were assembled on cold-mounted epoxy (see Figure 2d) and put in a fume hood for one night.
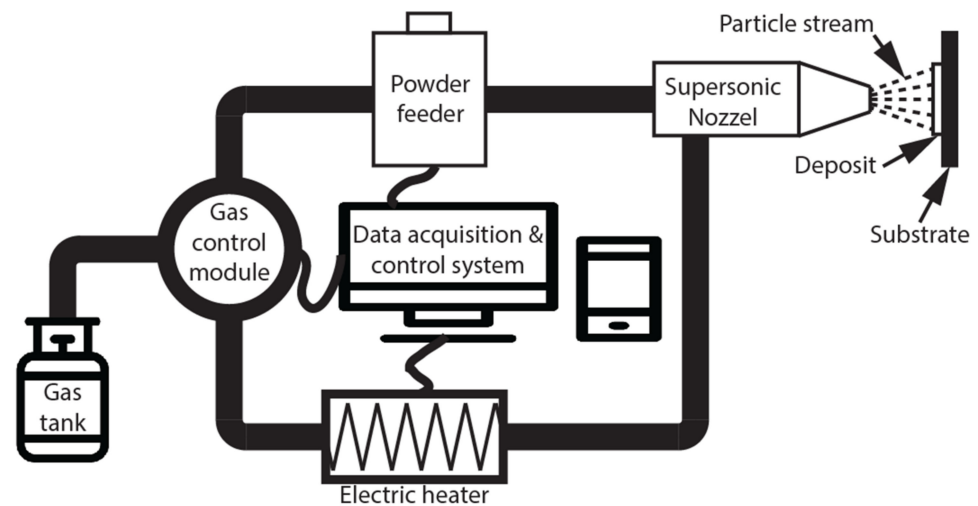
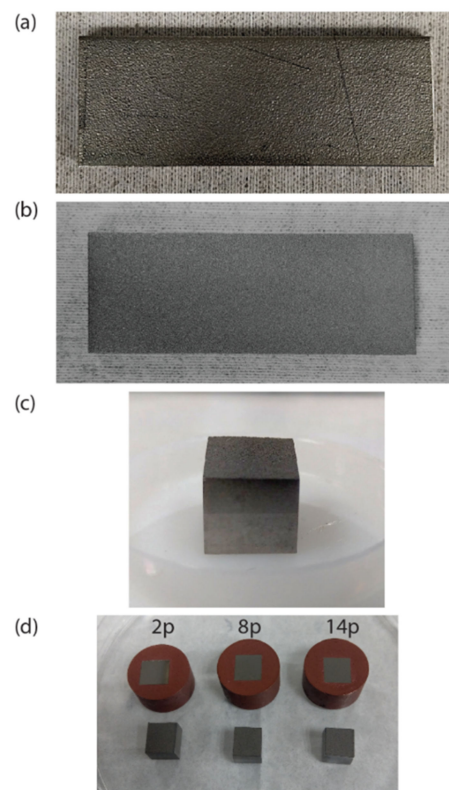

Figure 1. Schematic of the cold-spray technology.

Figure 2. Preparation of cold-sprayed Ti. (**a**) The Ti substrate after grit blasting and purging with pressurized air; (**b**) Ti substrate type of 2p after cold spray deposition; (**c**) A 1 cm³ Ti cube; (**d**) Mounted samples.

As obtained through SEM images of the study [1,21–23], the average diameter of the powder particles was about 25 μm. The surface roughness of cold-spray coating is very considerable. Therefore, it is necessary to roughen treatment to prepare for the next step. Before deposition of TiN thin film, the roughness of the Ti cold-spray coating is treated by grinding and polishing to allow more acceptable adhesion of the thin film and avoid

damage during deposition. The surface of Ti cold-spray coating was ground with the grinding papers mentioned in ref. [1]. In the next step, 9 μm, 3 μm, and 1 μm diamond suspensions were used to polish the test samples. Finally, any surface defects of the coating were treated using 10% hydrogen peroxide liquid and 0.05 μm colloidal silica.

2.2. TiN Thin Film HiPIMS Deposition

The TiN was coated employing HiPIMS during the deposition process; this experiment used the pulsed DC controller SPIK 2000A (Shen Chang Electric Co., LTD., New Taipei, Taiwan), which included two target guns in the vacuum chamber. The three-inch target gun was equipped with a pulsed power generator to satisfy the need to deposit thin films through HiPIMS. The target was connected to a HiPIMS power supply which was used in combination with a partial pressure of gas and using the nitrogen to grow the hard coatings. The schematic diagram of the HiPIMS system is described in Figure 3.
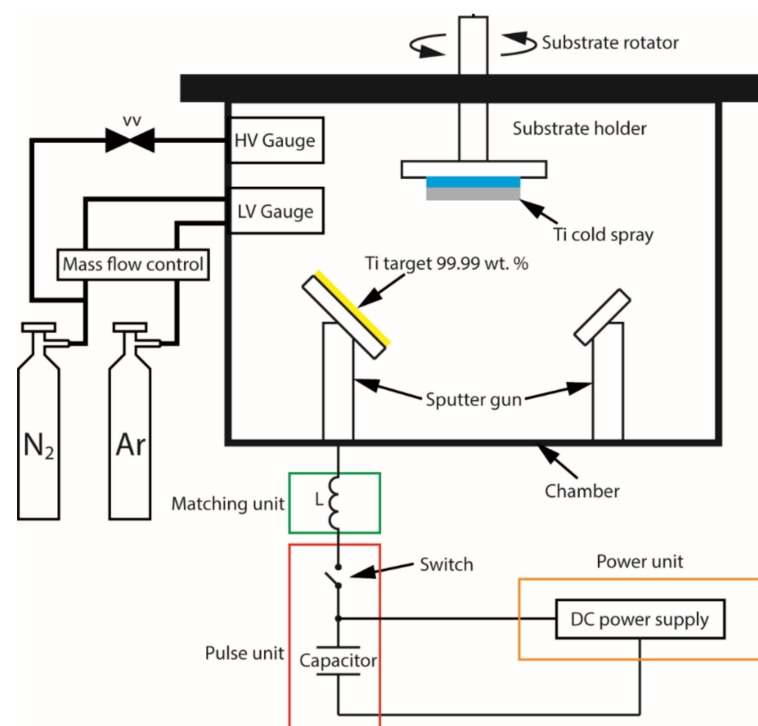

Figure 3. Schematic of the HiPIMS system.

Before the deposition, the Ti substrate from Ti cold spray samples was cleaned with acetone, isopropyl alcohol, and deionized water. The cleaning effect was enhanced with an ultrasonic oscillator during the cleaning process. In order to enhance the adhesion between TiN and Ti substrate, an ultrathin Ti adhesion film was deposited in between the cold spray coating and the TiN thin film [24–26]. Before sputtering, the experimental parameters were fixed, such as Deposition Distance = 80 mm, Substrate Rotation = 10 rpm, using 3 inches of Ti targets. First, the mechanical pump pumped until the pressure reached 5×10^{-3} Torr, and the cryogenic pump lowered the base pressure until the chamber reached 7.5×10^{-7} Torr. The TiN films were deposited, power was set at 150 W, the duty cycle of HiPIMS was set at (On-time 40 μs/Off time 360 μs), the working pressure was fixed at 5×10^{-3} Torr, the N_2/Ar flow rate was 3:18 sccm for the process, the Ti film power was set at 40 W, the duty cycle of HiPIMS set at (On-time 40 μs/Off time 40 μs), and the Ar flow rate was 18 sccm for the process. The target surface was pre-sputtered for 10 min, and the deposition time was calculated according to the deposition rate of the target to reach the required film thickness for the experiment. The process parameters are shown in Table 1. In the sputtering process, the first step is to use ion bombardment (40 W, 10 min) to clean the dust and oxide layer. The 50 nm Ti adhesion layer was deposited by HiPIMS, followed by a

600 nm TiN layer. Figure 4 shows TiN and Ti adhesion thin film deposition parameters deposited on Ti cold-spray coating.

Table 1. Information of TiN and Ti adhesion thin film deposited on the surface of cold-sprayed Ti.

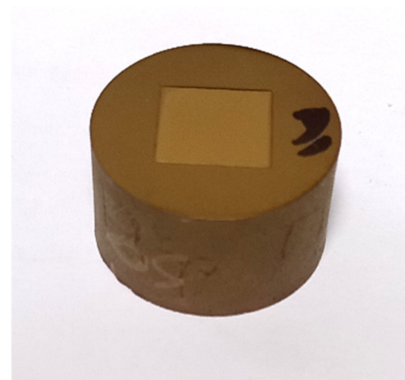| HiPIMS Conditions	TiN	Ti
Power (W)	150	40
Process Pressure (Torr)	5×10^{-3}	5×10^{-3}
On/off time (µs)	40/360	40/40
Time (min)	30	10
Rate of N_2:Ar gas (sccm)	3:18	0:18
Voltage (V)	550	404
Thickness (nm)	600	50

Figure 4. The mounted samples after deposition of TiN thin film.

2.3. Nano-Indentation Testing, Surface Profilometer and Atomic Force Microscope (AFM)

A nano-indenter was used to measure the modulus and the hardness of the cold-sprayed samples. For each sample, a 5-mN load indentation was performed on the surface with Hysitron Ubi3 (Hysitron Incorporated, Minneapolis, MN, USA).

A surface profiler was used to measure the profile of the surface roughness, surface texture, surface waviness, surface step height, and the deposited thin film thickness by contacting and scanning a sharp stylus with a very small measurement force (less than millinewtons). The line scanning of a stylus on a rough substrate surface can change the height of the stylus to be detected by a displacement sensor. Here, the surface profilometer test was carried out with Bruker DektakXT® (Bruker Co., Billerica, MA, USA). Atomic force microscopy (AFM) is a type of scanning probe microscopy (SPM) with a demonstrated resolution in the order of fractions of a nanometer which is more than 1000 times better than the optical diffraction limit. A mechanical probe gathers the information by "feeling" or "touching" the surface. Piezoelectric elements that facilitate tiny but accurate and precise movements on (electronic) command enable precise scanning.

2.4. FIB–DIC

The FIB ring-core milling process was performed using JEOL JIB-4601F (JEOL, Tokyo, Japan) following the residual stress measurement procedure from a previous study [19]. Here, the milling dose was 0.3, and the beam was set at 9 for the TiN/Ti duplex coating. The outside diameter was 5 µm, while the inside diameter was 2.5 µm. For each core, milling was conducted five times to reach the cold-spray Ti coating. According to ASTM E837, a diameter ratio of 0.5 yields a relatively uniform maximum stress release [27].

The milling was performed five times for each sample tested here, as shown in Figures 5 and 6. Figure 5 shows the milling process of each step in the samples. In samples, the first and the second rows show the images taken by angular SEM (Figure 6a–c), and the others show the images taken by horizontal SEM attached to FIB (Figure 6e,f), which had a bit lower resolution but did not pose a problem caused by the angle of the instrument.
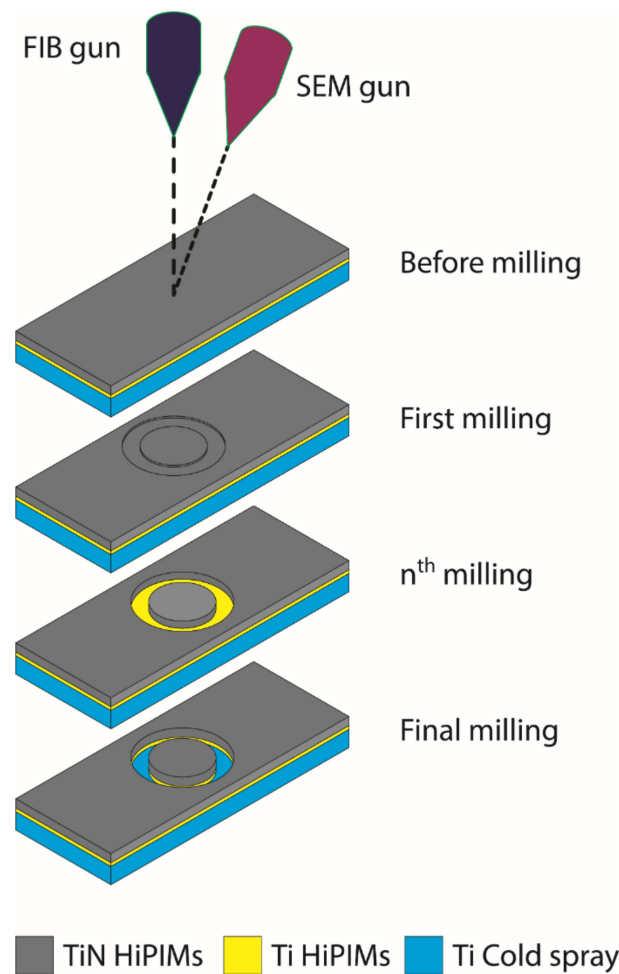
Figure 5. Schematic diagram of the the ring-core milling process.

2.5. Methods of Residual Stress Measurement

The the ring-core milling method was utilized to determine thin film's stress established on the transition of the surface core of deposited coatings. The three types of Ti cold-spray coating (multi passes: 2p, 8p, 14p) and dimensions of 5 mm (thickness) were used for this study. The TiN thin films with a thickness of 600 nm and Ti adhesion film with a thickness of 50 nm were deposited and used to study the influence of multi passes of the Ti cold-spray coating. The combined strain of the ring-core milling method can be calculated using [15]:

$$\varepsilon_P = \frac{\varepsilon_x + \varepsilon_y}{2} + \frac{\varepsilon_x - \varepsilon_y}{2} \cos 2\beta + \frac{1}{2}\gamma_{xy} \sin 2\beta, \tag{1}$$

$$\varepsilon_Q = \frac{\varepsilon_x + \varepsilon_y}{2} + \frac{\varepsilon_x - \varepsilon_y}{2} \cos 2(\beta + \varphi) + \frac{1}{2}\gamma_{xy} \sin 2(\beta + \varphi), \tag{2}$$

$$\varepsilon_R = \frac{\varepsilon_x + \varepsilon_y}{2} + \frac{\varepsilon_x - \varepsilon_y}{2} \cos 2(\beta + \varnothing) + \frac{1}{2}\gamma_{xy} \sin 2(\beta + \varnothing), \tag{3}$$

Equations (3)–(5) express the three strain values measured at the three different corners. Where ε_P, ε_Q, and ε_R are the strain values at the corners β on the *x*-axis, $(\beta + \varphi)$ and $(\beta + \varnothing)$. In this study, β, φ, and $\varnothing$ were assumed 0°, 45°, and 90°. The strain ε_y, γ_{xy}, and ε_y are taken by DIC analysis [15,28,29].

The stress can be calculated for a thin film by Equations (4) and (5):

$$\sigma_x = \frac{\varepsilon_P + \varepsilon_R}{4\overline{a}} + \frac{\sqrt{2}}{4\overline{b}}\sqrt{\left(\varepsilon_P - \varepsilon_Q\right)^2 + \left(\varepsilon_Q - \varepsilon_R\right)^2}, \tag{4}$$

$$\sigma_y = \frac{\varepsilon_P + \varepsilon_R}{4\overline{a}} - \frac{\sqrt{2}}{4\overline{b}}\sqrt{\left(\varepsilon_P - \varepsilon_Q\right)^2 + \left(\varepsilon_Q - \varepsilon_R\right)^2}, \tag{5}$$

where $\overline{a}$ and $\overline{b}$ are calibration coefficients follow ASTM E837 [27].
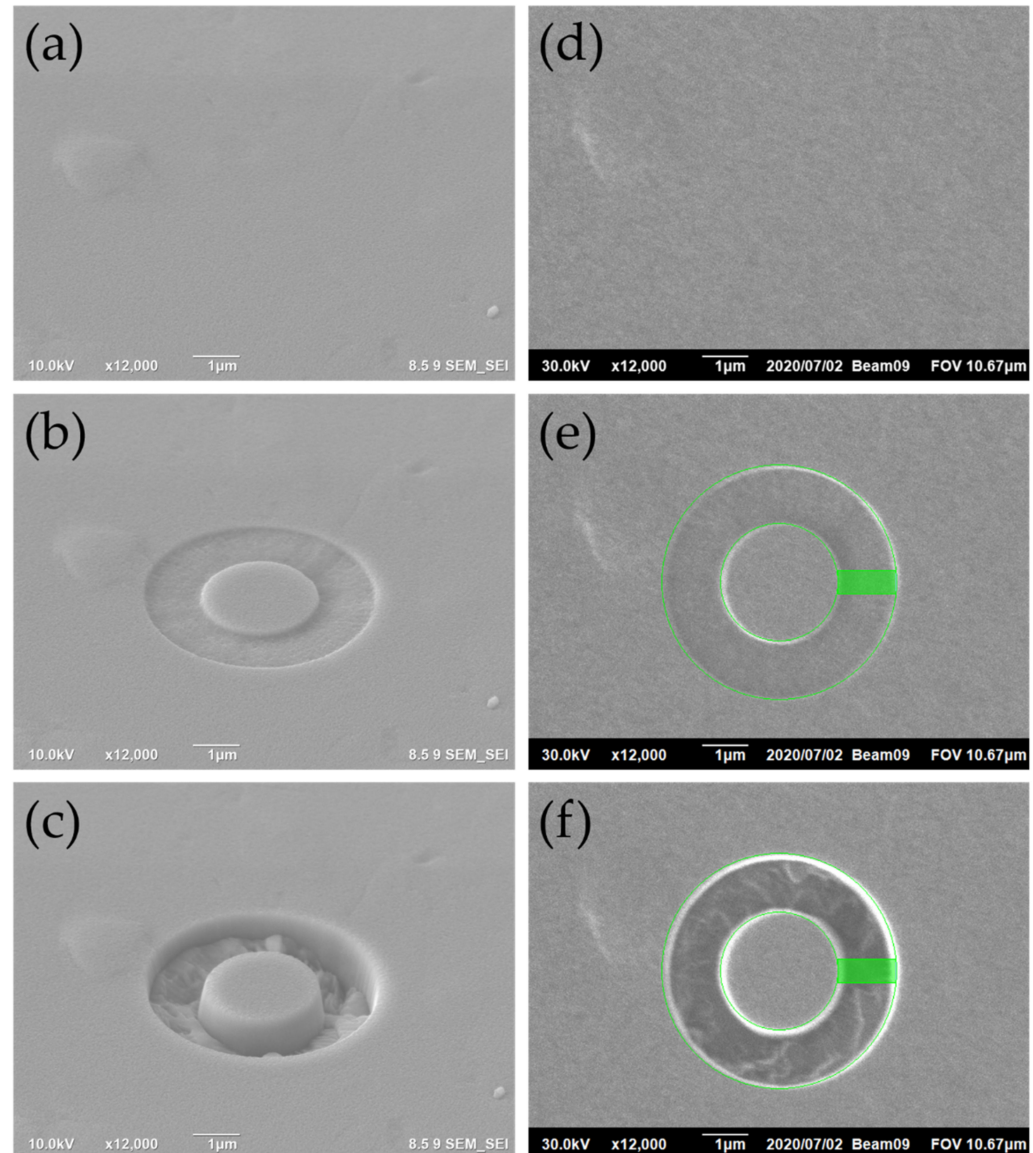

Figure 6. Images of TiN/Ti 8p sample: (**a**) Angular SEM image without milling, (**b**) Angular SEM image after 1st milling, (**c**) Angular SEM image after final milling, (**d**) Horizontal SEM image without milling, (**e**) Horizontal SEM image after 1st milling, and (**f**) Horizontal SEM image after final milling.

The the ring-core milling method yields a uniform strain and stress release, which is similar to concentric circles. In another study by Korsunsky et al. [17–19], because the noise was around the core, the DIC displacement/strain fields could be perfectly estimated around 60%–80% of the core diameter in the investigated area. In this study, the area was selected in the center of core Figure 7 of 81 × 81 pixels in size. In this case, the second-order fitting method was applied to the full-field displacement by using Matlab (2009, Natick, MA, USA) according to the research [15,28,29]. The SEM image drift, spatial distortion,

and magnification variations throughout the calibration protocol refer to our previous study [28]. The strain release was approached to the concentric circles.
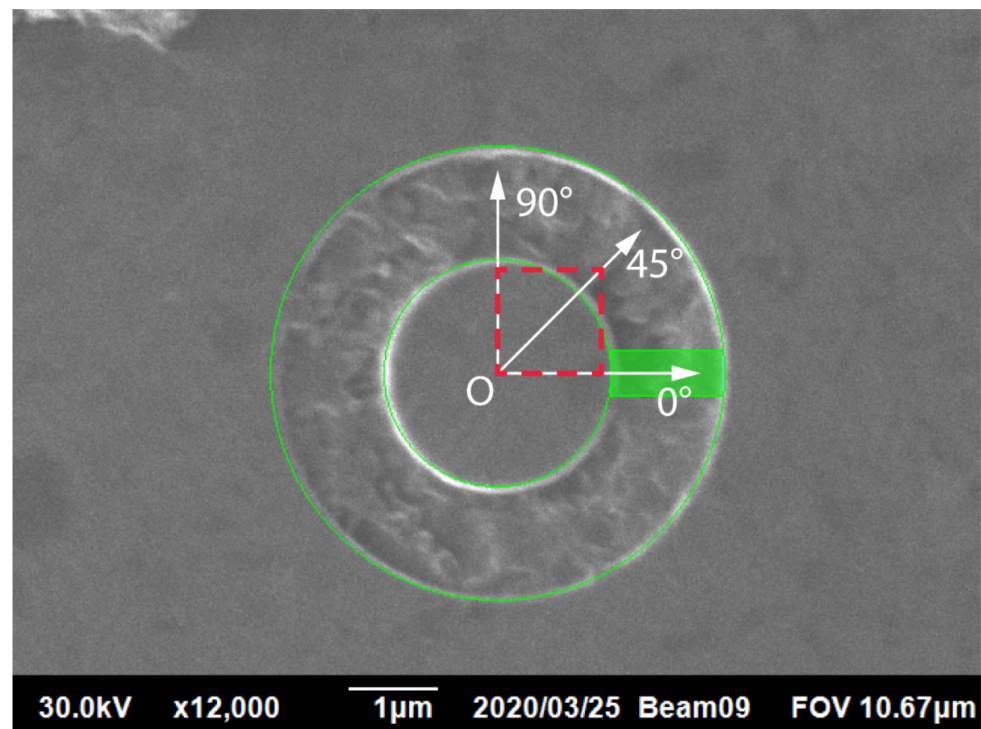

Figure 7. The quarter area which was selected to calculate the residual stress by THE FIB–DIC method.

3. Results and Discussion

3.1. Roughness and Hardness Measurement

After polishing, the surface of the cold-spray coat should be inspected by AFM. In the AFM test, the roughness of the Ti 2p, 8p, and 14p blocks before roughening treatment were 7.58, 10.03, and 12.66 µm. After grinding and polishing, the roughness of each sample is shown in Figure 8 and the average roughness was 1.88, 1.07, and 1.3 nm. Since the surface roughness values of the block samples were almost the same, the adhesion between HiPIMS thin film and Ti cold spray was enhanced. The SEM images and grain-size distribution on the surface of TiN on 8p Ti cold-spray coating deposited by HiPIMS technology are exhibited in Figure 9. As obtained through SEM images, the size and distribution of the particles were very uniform, demonstrating that the surface roughness of the 8p sample was excellent. In Figure 10, the surface roughness result of TiN was 4.31, 1.58, and 3.82 nm.
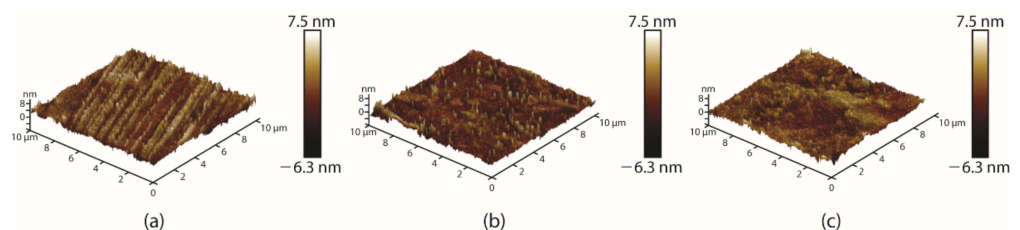

Figure 8. AFM test of Ti cold-spray samples after grinding and polishing: (**a**) 2p, (**b**) 8p, and (**c**) 14p.

The nano-indentation test was performed on the Ti cold spray and HiPIMS TiN thin film to obtain Young's modulus, which was then used to calculate the residual stress. For the cold-spray Ti, Young's modulus measured by the indentation was within the normal range for Ti 2p, 8p, and 14p and varied between 106 GPa and 114.5 GPa. The hardness of Ti cold spray samples ranged from 2.4 GPa to 2.8 GPa (Table 2). The Ti cold spray 2p

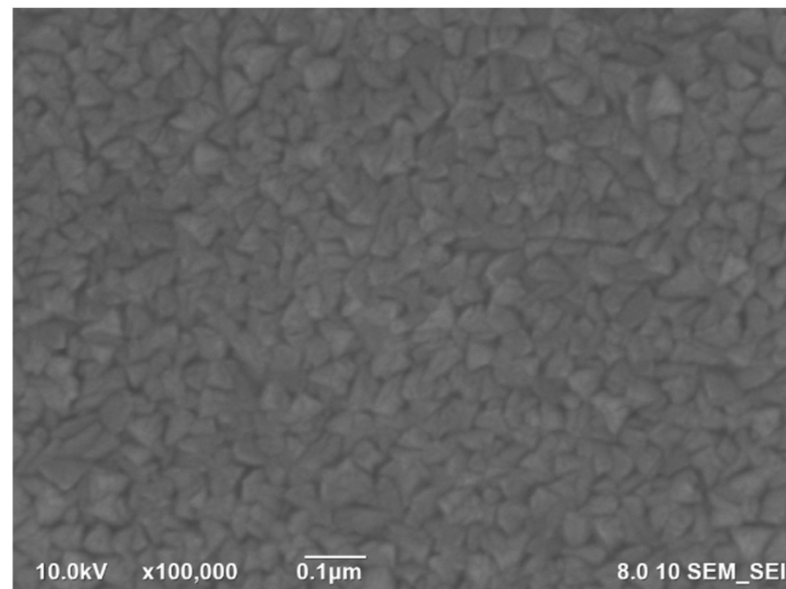had the deepest indentation depth, but the Ti cold spray 8p had the highest hardness and Young's modulus.

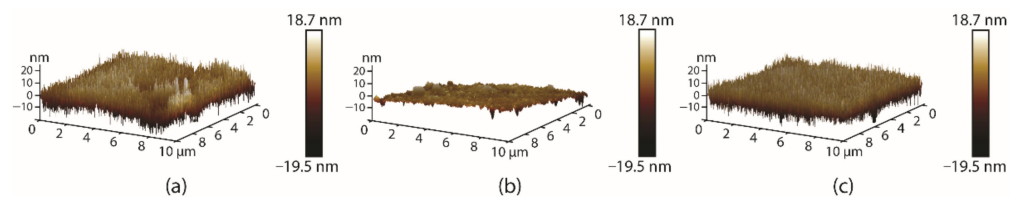**Figure 9.** SEM images showing grain size and morphology of TiN/Ti 8p thin film.

Figure 10. Roughness of TiN thin film on cold-spray Ti samples: (**a**) 2p, (**b**) 8p, and (**c**) 14p.

Table 2. Nano-indentation results of Ti cold spray samples.

Sample	Modulus (GPa)	Hardness (GPa)
Ti 2p	113.10 ± 9.63	2.405 ± 0.2
Ti 8p	114.26 ± 8.95	2.74 ± 0.29
Ti 14p	106.54 ± 12.81	2.68 ± 0.26

For the TiN/Ti samples, Figure 11, show the displacement-load curve recorded using the nanoindentation technique. Young's modulus computed by the nanoindentation method was within the normal range for TiN/Ti 2p, 8p, and 14p, and varied between 159 GPa and 183 GPa. The hardness ranged from 21 GPa to 22 GPa (see Table 3). The hardness results were reflected in the indentation depth. The TiN/Ti 8p sample had the lowest concavity indentation depth and the highest hardness.

Table 3. Nano-indentation result of TiN/Ti samples.

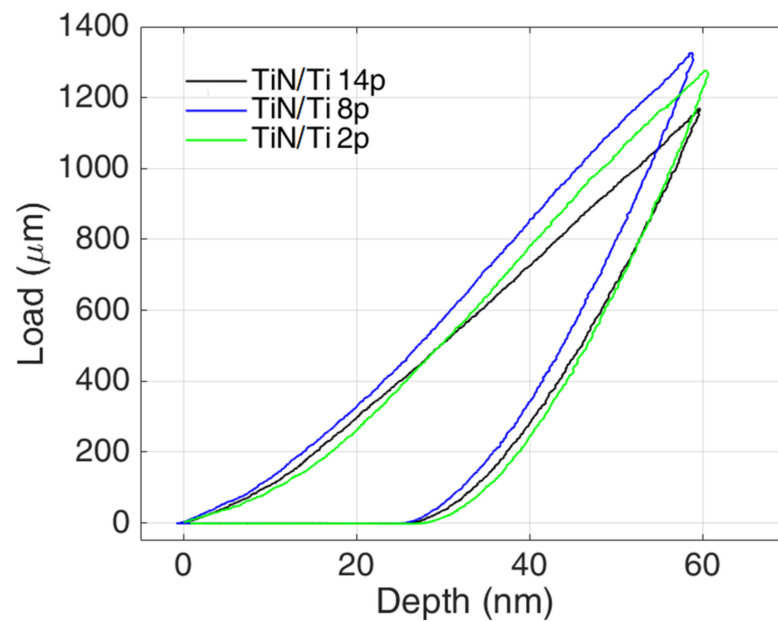| Sample	Modulus (GPa)	Hardness (GPa)
TiN/Ti 2p	167.35 ± 5.64	21.36 ± 1.13
TiN/Ti 8p	182.68 ± 8.98	21.96 ± 0.87
TiN/Ti 14p	159.24 ± 6.75	21.67 ± 0.50

Figure 11. Load versus depth-load of TiN/Ti samples.

3.2. DIC Displacement and Strain Measurement

Figure 12 shows the depth-strain release of TiN/Ti 14p samples using full-field measurements of the surface deformation performed by DIC the technique [15]. The area was selected to calculate the residual stress (see Figure 7). The resulting depth–strain release of the 2p and 8p samples also had the same line profile as Figure 12. The ε_x, γ_{xy}, and ε_y were depth–strain distribution values obtained at different milling depths after measuring surface strain by DIC analysis [15,28,29]. The depth–strain distribution data were calculated with a 50 nm depth step. The depth–strain distribution fitting curves were used in Formulas (1)–(3) to calculate the combined strain ε_P, ε_Q, and ε_R.
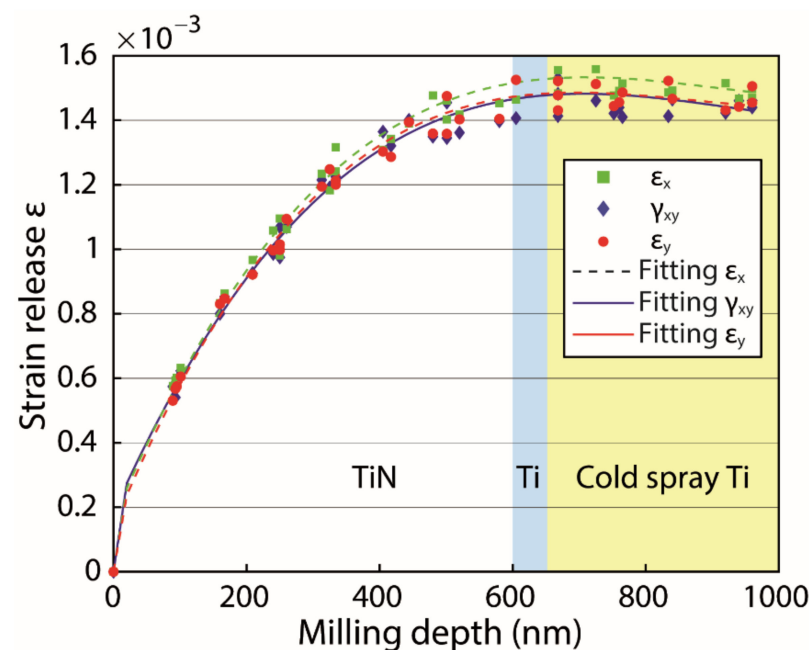

Figure 12. The depth–strain release curves of TiN/Ti 14p.

3.3. Residual Stress of TiN Thin Film and TiN/Ti Duplex Coating

　　The residual stress result of TiN thin film and TiN/Ti duplex coating were obtained by applying the Formulas (4) and (5) with FEA calculated calibration coefficients corresponding to the materials properties of TiN and Ti. As shown in Figure 13, the relaxed residual stress of the TiN/Ti duplex coating measured by the FIB–DIC increased from the surface to a depth of 0 to 600 nm and converged from the depth of 600 to 1000 nm. (Noted the thickness of TiN is 600 nm and Ti adhesion layer is 50 nm). It appears the residual stress was majorly exerted within the TiN cap layer and remained steady as the milling depth went through the Ti adhesion layer and the Ti cold-spray coating. The residual stress relaxed deeply within the TiN layer and the maximum residual stress of 2p, 8p, and 14p samples were 3500.4 MPa, 4316 MPa, and 4041.8 MPa, respectively, which were located nearly above the interface of TiN/Ti. As shown in the Figure, the relaxation stress of three different samples did not show significant differences despite the TiN/Ti 8p having the highest value. When the milling depth passed through the Ti adhesion layer to over a depth of 650 nm, the residual stress release tended to stall. This result indicates there was very little residual stress remaining within the cold-spray Ti layer.
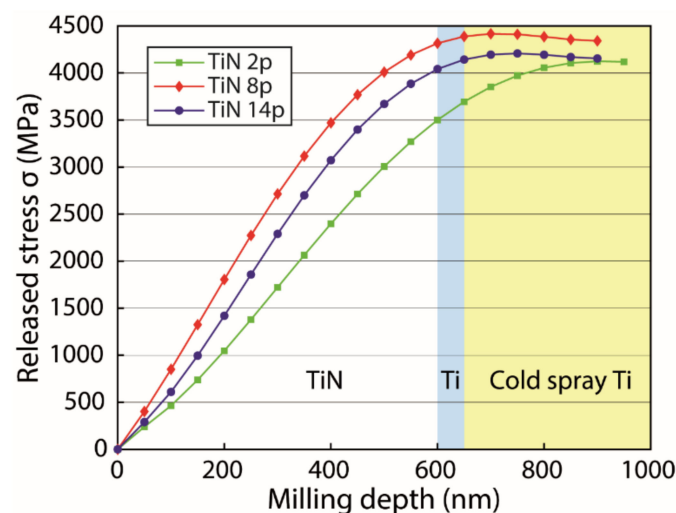

Figure 13. The residual stress result of TiN/Ti duplex coating: TiN 2p, TiN 8p, and TiN 14p.

3.4. Discussion

　　The roughness results of Ti cold-spray coating obtained from Section 3.1 show that after the grinding and polishing process, the surfaces of the samples were entirely similar. This smoothness on the surface roughness of the sample will therefore enhance the deposition process of TiN using HiPIMS. Regarding the mechanical properties such as Young's modulus, hardness, and roughness of TiN thin film and cold-spray Ti, the values were shown as consistent with those of others [1,3,21,22]. Since the HiPIMS TiN thin film deposition used the same process parameters for all three different cold-spray samples, it may be suggested that the mechanical properties of the cold-spray coating substrate could be the determining factor for the mechanical properties of TiN/Ti duplex coating. A previous study on the number of passes for cold-spray fabrication [30] reported that the case with two passes gave higher hardness than three passes or one pass. That means as the number of passes increases, the hardness of the cold-spray coating will steadily improve or reduce. That may be why the cold spray sample of 8p had higher hardness than 14p and 2p. As shown in Tables 2 and 3, the cold-spray Ti 8p sample had the highest hardness and Young's modulus, resulting in the highest value of TiN/Ti 8p duplex coating sample.

　　As illustrated in Figure 6, the core was generated using FIB without the protection ring [23]. In Figure 6f, the study presented a rounded edge around the core. That proves that selecting the strain field measurement area is especially necessary. The ring core method is applied on the surface of thin film, and equivalent biaxial stress of the plane

is used for analysis [15,17]. Calibration coefficients can be used according to standard protocol [26] to obtain residual stresses. The residual stress of the FIB–DIC measurement showed that the residual stress difference of these three different samples was close (about 5%–7%) together, with the milling depth reaching over 800 nm. By closely examining the residual stress at a depth of 650 nm (near the interface between TiN and Ti), TiN/Ti 14p and TiN/Ti 8p are observed to have higher residual stress than TiN/Ti 2p, in which the residual stress of the sample 14p reached 4143 MPa while sample 8p had a residual stress of 4338.6 MPam indicating the TiN/Ti 8p had the highest residual stress.

As shown in Figure 13, the residual stress relaxed drastically from the surface to the milling depth of 0 to 600 nm and converged from 600 to 1000 nm. The residual stress mostly remained within the hard coating of TiN and remained minimal inside the Ti cold-spray coating. We found that the cold-spray coating did not exert too much stress on all the tested TiN/Ti duplex coating samples. Previously, the study showed Ti cold-spray coating with a thickness more sumptuous than 1 mm. Residual stress did not exceed 100 MPa [31]. When the thickness reached 5 mm, the residual stress of cold-spray Ti was approximately 20 MPa [32]. Consequently, the dissimilarity of our study in residual stress of Ti 2p, 8p, and 14p cold spray coatings is nearly the same. In view of this, the residual stress of the TiN thin film is attributed to not being notably altered by the Ti cold-spray coating substrate.

In general, the hardness of the cold-spray Ti coatings 2p, 8p, and 14p were very similar (shown in Table 2). In Table 3, the TiN thin film was deposited on cold spray-coatings and the hardness of the samples increased by nine times. The results indicated that the TiN/Ti 8p duplex coating has superior properties in terms of hardness, roughness, and Young's modulus but has the largest residual stress. The TiN/Ti 2p duplex coating can still be used in industrial production due to characteristics such as short fabrication time and minimal residual stress, although it has a slight disadvantage in hardness and roughness of the surface. It is worth noting that without the TiN cap thin film, Ti 2p cold spray can cause severe damage if not detected in time. The TiN/Ti 14p duplex coating has better mechanical properties than the TiN/Ti 2p duplex sample and has less residual stress than the TiN/Ti 8p duplex sample, but it is more time-consuming and expensive to fabricate than other samples.

4. Conclusions

This study provided detailed information on the hardness, roughness, material properties, and residual stresses of HiPIMS TiN thin films deposited on cold-sprayed Ti coatings by AFM, nano-indentation, SEM, and FIB–DIC. The HiPIMS deposition of thin film does have very high hardness. SEM and AFM experiments showed that HIPIMS-TiN/Ti had a dense nanostructure and a perfectly smooth surface. The residual stress mostly remained within the hard coating of TiN and very little was inside the Ti cold-spray coating. We found that the cold-spray coating did not exert too much stress on all the tested TiN/Ti thin film samples. In contrast, the residual stress of the HiPIMS thin films were higher but did not damage the cold-spray coating because the thickness of the cold-spray Ti coating is very thick. Simultaneously, the residual stresses values of duplex coatings obtained from this study provided very useful information with the load capacity to prevent failure of coatings and can be used to predict their life cycle. For Ti cold-spray coating, as the number of passes increases, the hardness of the cold-spray coating will steadily improve or reduce. The cold-spray Ti 8p sample had the highest hardness and Young's modulus, which could result in the highest value of TiN/Ti 8p duplex coating sample. The TiN/Ti 2p duplex coating had short fabrication time, minimal residual stress, although a slight disadvantage in hardness and roughness of surface. The TiN/Ti 14p duplex coating had better mechanical properties than the TiN/Ti 2p duplex sample and had less residual stress than that of the TiN/Ti 8p duplex coating sample.

References

1. Goldbaum, D.; Manimuda, P.; Kamath, G.; Descartes, S.; Klemberg-Sapieha, J.E.; Chromik, R.R. Tribological behavior of TiN and Ti (Si,C)N coatings on cold sprayed Ti substrates. *Surf. Coat. Technol.* **2016**, *291*, 264–275. [CrossRef]
2. Fardan, A.; Berndt, C.C.; Ahmed, R. Numerical modelling of particle impact and residual stresses in cold sprayed coatings: A review. *Surf. Coat. Technol.* **2021**, *409*, 126835. [CrossRef]
3. Alidokht, S.A.; Vo, P.; Yue, S.; Chromik, R.R. Cold Spray Deposition of Ni and WC-Reinforced Ni Matrix Composite Coatings. *J. Therm. Spray Technol.* **2017**, *109*, 1908–1921. [CrossRef]
4. Walker, M. Microstructure and bonding mechanisms in cold spray coatings. *Mater. Sci. Technol.* **2018**, *34*, 2057–2077. [CrossRef]
5. Wong, W.; Irissou, E.; Ryabinin, A.N.; Legoux, J.G.; Yue, S. Influence of helium and nitrogen gases on the properties of cold gas dynamic sprayed pure titanium coatings. *J. Therm. Spray Technol.* **2011**, *20*, 213–226. [CrossRef]
6. Kouznetsov, V.; Macák, K.; Schneider, J.M.; Helmersson, U.; Petrov, I. A novel pulsed magnetron sputter technique utilizing very high target power densities. *Surf. Coat. Technol.* **1999**, *122*, 290–293. [CrossRef]
7. Ehiasarian, A.P.; New, R.; Münz, W.D.; Hultman, L.; Helmersson, U.; Kouznetsov, V. Influence of high power densities on the composition of pulsed magnetron plasmas. *Vacuum* **2002**, *65*, 147–154. [CrossRef]
8. Helmersson, U.; Lattemann, M.; Bohlmark, J.; Ehiasarian, A.P.; Gudmundsson, J.T. Ionized physical vapor deposition (IPVD): A review of technology and applications. *Thin Solid Films* **2006**, *513*, 1–24. [CrossRef]
9. Kubart, T.; Čada, M.; Lundin, D.; Hubička, Z. Investigation of ionized metal flux fraction in HiPIMS discharges with Ti and Ni targets. *Surf. Coat. Technol.* **2014**, *238*, 152–157. [CrossRef]
10. Čapek, J.; Hála, M.; Zabeida, O.; Klemberg-Sapieha, J.E.; Martinu, L. Steady state discharge optimization in high-power impulse magnetron sputtering through the control of the magnetic field. *J. Appl. Phys.* **2012**, *111*, 23301. [CrossRef]
11. Hála, M.; Čapek, J.; Zabeida, O.; Klemberg-Sapieha, J.E.; Martinu, L. Pulse management in high power pulsed magnetron sputtering of niobium. *Surf. Coat. Technol.* **2012**, *206*, 4186–4193. [CrossRef]
12. Ehiasarian, A.P.; Hovsepian, P.E.; Hultman, L.; Helmersson, U. Comparison of microstructure and mechanical properties of chromium nitride-based coatings deposited by high power impulse magnetron sputtering and by the combined steered cathodic arc/unbalanced magnetron technique. *Thin Solid Films* **2004**, *457*, 270–277. [CrossRef]
13. Hultman, L.; Sundgren, J.E.; Greene, J.; Bergstrom, D.; Petrov, I. High-flux low-energy ($\approx$20 eV) N+ 2 ion irradiation during TiN deposition by reactive magnetron sputtering: Effects on microstructure and preferred orientation. *J. Appl. Phys.* **1995**, *78*, 5395–5403. [CrossRef]
14. Chen, W.-C.; Wang, Z.-Y.; Yu, C.-Y.; Liao, B.-H.; Lin, M.-T. A study of the phase transformation of low temperature deposited tantalum thin films using high power impulse magnetron sputtering and pulsed DC magnetron sputtering. *Surf. Coat. Technol.* **2022**, *436*, 128288. [CrossRef]
15. Chen, T.Y.-F.; Chou, Y.-C.; Wang, Z.-Y.; Lin, W.-Y.; Lin, M.-T. Using Digital Image Correlation on SEM Images of Strain Field after Ion Beam Milling for the Residual Stress Measurement of Thin Films. *Materials* **2020**, *13*, 1291. [CrossRef]
16. Sebastiani, M.; Eberl, C.; Bemporad, E.; Pharr, G.M. Depth-resolved residual stress analysis of thin coatings by a new FIB–DIC method. *Mater. Sci. Eng. A* **2011**, *528*, 7901–7908. [CrossRef]
17. Korsunsky, A.M.; Sebastiani, M.; Bemporad, E. Focused ion beam ring drilling for residual stress evaluation. *Mater. Lett.* **2009**, *63*, 1961–1963. [CrossRef]
18. Korsunsky, A.M.; Salvati, E.; Lunt, A.G.J.; Sui, T.; Mughal, M.Z.; Daniel, R.; Keckes, J.; Bemporad, E.; Sebastiani, M. Nanoscale residual stress depth profiling by Focused Ion Beam milling and eigenstrain analysis. *Mater. Des.* **2018**, *145*, 55–64. [CrossRef]
19. Korsunsky, A.M.; Sebastiani, M.; Bemporad, E. Residual stress evaluation at the micrometer scale: Analysis of thin coatings by FIB milling and digital image correlation. *Surf. Coat. Technol.* **2010**, *205*, 2393–2403. [CrossRef]
20. ASTM International, ASTM B265-20a. Available online: https://www.astm.org/b0265-20a.html (accessed on 9 April 2022).

21. Ajaja, J.; Goldbaum, D.; Chromik, R.R. Characterization of Ti cold spray coatings by indentation methods. *Acta Astronaut.* **2011**, *69*, 923–928. [CrossRef]

22. Goldbaum, D.; Ajaja, J.; Chromik, R.R.; Wong, W.; Yue, S.; Irissou, E.; Legoux, J.G. Mechanical behavior of Ti cold spray coatings determined by a multi-scale indentation method. *Mater. Sci. Eng. A* **2011**, *530*, 253–265. [CrossRef]

23. Goldbaum, D.; Chromik, R.R.; Brodusch, N.; Gauvin, R. Microstructure and Mechanical Properties of Ti Cold-Spray Splats Determined by Electron Channeling Contrast Imaging and Nanoindentation Mapping. *Microsc. Microanal.* **2015**, *21*, 570–581. [CrossRef] [PubMed]

24. Wang, Z.; Zhang, D.; Ke, P.; Liu, X.; Wang, A. Influence of Substrate Negative Bias on Structure and Properties of TiN Coatings Prepared by Hybrid HIPIMS Method. *J. Mater. Sci. Technol.* **2015**, *31*, 37–42. [CrossRef]

25. Elmkhah, H.; Attarzadeh, F.; Fattah-alhosseini, A.; Kim, K.H. Microstructural and electrochemical comparison between TiN coatings deposited through HIPIMS and DCMS techniques. *J. Alloys Compd.* **2018**, *735*, 422–429. [CrossRef]

26. Lei, S.; Huang, J.-H.; Chen, H. Measurement of residual stress on TiN/Ti bilayer thin films using average X-ray strain combined with laser curvature and nanoindentation methods. *Mater. Chem. Phys.* **2017**, *199*, 185–192. [CrossRef]

27. ASTM International, ASTM E837-08. Available online: https://www.astm.org/e0837-08.html (accessed on 9 April 2022).

28. Chen, T.Y.-F.; Chen, T.-C.; Cheng, F.-Y.; Tsai, A.-T.; Lin, M.-T. Digital image correlation of SEM images for surface deformation of CMOS IC. *Microelectron. Eng.* **2018**, *201*, 16–21. [CrossRef]

29. Chen, T.Y.-F.; Dang, N.M.; Wang, Z.-Y.; Chang, L.-W.; Ku, W.-Y.; Lo, Y.-L.; Lin, M.-T. Use of Digital Image Correlation Method to Measure Bio-Tissue Deformation. *Coatings* **2021**, *11*, 924. [CrossRef]

30. Moridi, A.; Gangaraj, S.M.H.; Vezzu, S.; Guagliano, M. Number of Passes and Thickness Effect on Mechanical Characteristics of Cold Spray Coating. *Procedia Eng.* **2014**, *74*, 449–459. [CrossRef]

31. Suhonen, T.; Varis, T.; Dost, S.; Torrell, M.; Guilemany, J.M. Residual stress development in cold sprayed Al, Cu and Ti coatings. *Acta Mater.* **2013**, *61*, 6329–6337. [CrossRef]

32. Luzin, V.; Kirstein, O.; Zahiri, S.H.; Fraser, D. Residual Stress Buildup in Ti Components Produced by Cold Spray Additive Manufacturing (CSAM). *J. Therm. Spray Tech.* **2020**, *29*, 1498–1507. [CrossRef]